Nanoscale

PAPER

View Article Online
View Journal

Cite this: DOI: 10.1039/c9nr06941k

Plant-derived chlorophyll derivative loaded liposomes for tri-model imaging guided photodynamic therapy†

Hailin Zhou,‡[a,b] Lu Xia,‡[b] Jing Zhong,[b] Saisai Xiong,[b] Xuan Yi,[b] Lei Chen,[c] Ran Zhu,*[b] Quanliang Shi*[a] and Kai Yang *[b]

Received 12th August 2019,
Accepted 8th October 2019

DOI: 10.1039/c9nr06941k

rsc.li/nanoscale

Plant-derived chlorophyll derivatives with a porphyrin ring structure and intrinsic photosynthesis have been widely used in biomedicine for cancer theranostics. Owing to their poor water solubility, chlorophyll derivatives are very difficult to use in biomedical applications. In this work, pyropheophorbide acid (PPa) (liposome/PPa) nanoparticles, a liposome-encapsulated chlorophyll derivative, are designed for tri-model imaging guided photodynamic therapy (PDT) of cancer. The obtained liposome/PPa nanoparticles significantly enhance the water solubility of PPa, prolong blood circulation and optimize the bio-distribution in mice after intravenous injection. Utilizing their intrinsic fluorescence, high near-infrared (NIR) absorbance and extra radiolabeling, liposome/PPa nanoparticles could be used as excellent contrast agents for multi-modal imaging including fluorescence (FL) imaging, photoacoustic (PA) imaging and SPECT/CT imaging. Under 690 nm laser irradiation at a low power density, liposome/PPa nanoparticles significantly inhibit tumor growth, further demonstrating the therapeutic efficiency of PDT using PPa. Therefore, our work developed liposome/PPa nanoparticles as multifunctional nanoagents for multimodal imaging guided PDT of cancer. This will further prompt the clinical applications of PPa in the future.

Introduction

As an important source of multi-pathway anticancer therapy, compounds extracted from natural plants have been at the forefront of current research.[1–3] Due to their pleiotropy, low toxicity and biocompatibility compared with anticancer drugs, pure natural plant extracts such as taxol[4–6] and vincristine[7,8] play an important role in the prevention and treatment of cancer.[9] As a kind of pure natural plant extract, chlorophyll and its derivatives are widely used to elucidate the photosynthesis mechanism, photochemical devices and photodynamic therapy (PDT) of cancer.[10] A series of chlorophyll-a derivatives, such as verteporfin,[11] Npe6,[12,13] radachlorins,[11] and HPPH,[14–16] have been licensed for clinical PDT by the Food and Drug Administration (FDA).[17] Pyropheophorbide a (PPa),[13,18] a product that comes from the degradation of chlorophyll, found in terrestrial and marine plants, and insect fluids, has been widely used as a highly potent photosensitizer for tumor imaging and PDT.[19] Using 690 nm laser irradiation, PPa could be activated for excellent *in vivo* fluorescence imaging and PDT of tumors. Unfortunately, similar to other photosensitizers, PPa exhibits considerable lipophilicity and planar conformation, resulting in its limited tumor targeting ability.[20,21] Therefore, such poor water solubility of PPa would induce the damage of normal tissues. Zheng and co-workers reported that a large amount of pyrophosphate was successfully bound to the liposome membranes. After loading into the lipid membranes, the absorption peak of chlorophyll derivatives is red-shifted. Additionally, as a metabolite of hemoglobin, the main porphyrin structure of PPa could be degraded from old red blood cells into bile pigment and excreted in feces.[22] Therefore, PPa is mainly degraded in the liver, converted into bile pigment and excreted from the body with feces, causing no harm to the human body and the external environment. Utilizing their intrinsic biological safety and environmental protection characteristics, chlorophyll derivatives could be applied as fluorescent reagents and photosensitizers. As a type of chlorophyll derivative, pyropheophorbide a

[a]School of Biology & Basic Medical Science, Medical College, Soochow University, Suzhou, Jiangsu 215123, China. E-mail: shiquanliang@suda.edu.cn
[b]State Key Laboratory of Radiation Medicine and Protection, School of Radiation Medicine and Protection and Interdisciplinary Sciences (RAD-X), Collaborative Innovation Center of Radiation Medicine of Jiangsu Higher Education Institutions, Soochow University, Suzhou, Jiangsu 215123, China. E-mail: kyang@suda.edu.cn, zhuran@suda.edu.cn
[c]The Affiliated Suzhou Hospital of Nanjing Medical University, Suzhou, Jiangsu 215001, China

†Electronic supplementary information (ESI) available. See DOI: 10.1039/c9nr06941k

‡These authors contributed equally to this work.

(PPa) could be used as an excellent contrast agent for imaging and as a photosensitizer for PDT of cancer, realizing imaging guided PDT.

In recent years, nanotechnology has been widely applied in nanomedicine including the diagnosis and treatment of cancer.[23,24] The use of nanomaterial based drug delivery could significantly enhance drug accumulation in the lesion, and decrease the side effects in treated patients.[25–27] Liposomes as typical nanocarriers have been widely applied for drug delivery, owing to their low toxicity, high biocompatibility and biodegradability, as well as long-time blood circulation.[28]

In this work, we selected liposomes as the nanocarriers to load PPa into the middle of the phospholipid bilayer, yielding liposome/PPa nanoparticles. Owing to the introduction of liposomes, the biocompatibility of the loaded PPa was significantly improved. From *in vitro* experiments, liposome/PPa nanoparticles exhibited excellent therapeutic efficiency against cancer cells under 690 nm laser irradiation. Importantly, the PPa-loaded liposomes showed long-term blood circulation and high tumor uptake after intravenous injection. Utilizing their intrinsic fluorescence, high NIR absorbance and extra radiolabelling, liposome/PPa nanoparticles could act as contrast agents for multimodal imaging including fluorescence imaging/photoacoustic (PA) imaging/SPECT imaging. Under 690 nm laser irradiation at a low power density, liposome/PPa nanoparticles significantly inhibited tumor growth compared with other control groups, further demonstrating the therapeutic efficiency of PDT with PPa. Therefore, our work developed liposome/PPa nanoparticles as multifunctional nanoagents for multimodal imaging guided PDT of cancer. This will further prompt the clinical applications of PPa in the future.

Results and discussion

In this work, liposome/PPa nanoparticles were synthesized by the following method. Utilizing the hydrophobic properties of PPa, it could be loaded into the phospholipid bilayer of the liposome (Scheme 1). The details of the synthesis process are provided in the Experimental section. The yields of liposome/PPa nanoparticles have been characterized in detail. Transmission electron microscopy (TEM) images showed that the as-prepared liposome/PPa nanoparticles were spherical with an average size of 100 nm (Fig. 1a). The hydrodynamic diameter of liposome/PPa was found to be 100–120 nm by dynamic light scattering (DLS) assay (Fig. 1b), further matching the TEM imaging data. Upon being incubated in different liquids including pure water, phosphate buffered saline (PBS), and cell culture medium DMEM with 10% fetal bovine serum (FBS) for 72 h, liposome/PPa nanoparticles show negligible fluctuations in their size (Fig. S1†). Owing to the PPa loading, the typical absorption peak of PPa was observed in the UV spectrum of the liposome/PPa nanoparticles and this could be used for measuring the PPa loading of liposomes at different input masses of PPa (Fig. 1d and Fig. S2†). After the addition of PPa, self-agglomeration of PPa took place inducing an absorption red shift at 710 nm. The agglomeration can be dispersed by ultrasound at 100 w for 30 min. The excitation and emission wavelengths of liposome/PPa were 450 nm and 690 nm, respectively (Fig. S3†). Considering the optical properties and high NIR absorbance, liposome/PPa nanoparticles could be applied for both fluorescence imaging and photoacoustic (PA) imaging. The PA imaging of liposome/PPa nanoparticles with different concentrations was tested using a Visualsonics Vevo 2100 LAZR PA imaging system, which showed that the PA signal strength of liposome/PPa was linearly related to the concentration (Fig. 1d). In order to demonstrate the properties of singlet oxygen ($^1O_2$) generated by PPa under laser irradiation, the $^1O_2$ sensor (SOSG) was used as a probe to prove that $^1O_2$ could be generated by the exposure of PPa to a 690 nm laser (at the power of 500 mW cm^{-2}) for predetermined time points of 0.5, 1.5, 2, 3, 5, 6, and 8 min (Fig. 1e). Therefore, liposome/PPa nanoparticles could be used for photodynamic therapy (PDT). In addition, utilizing the

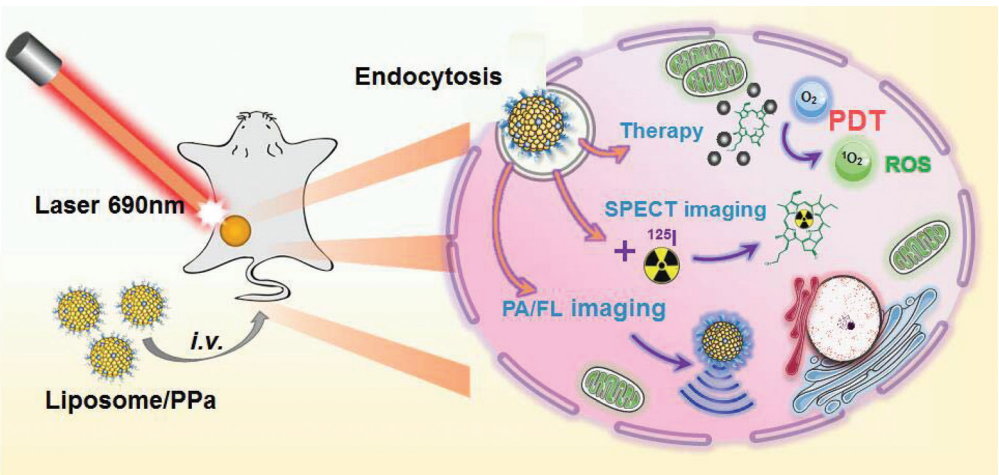

Scheme 1 Schematic illustration to show the fabrication process of liposome/PPa and *in vivo* tumor multimodal imaging and photodynamic therapy.

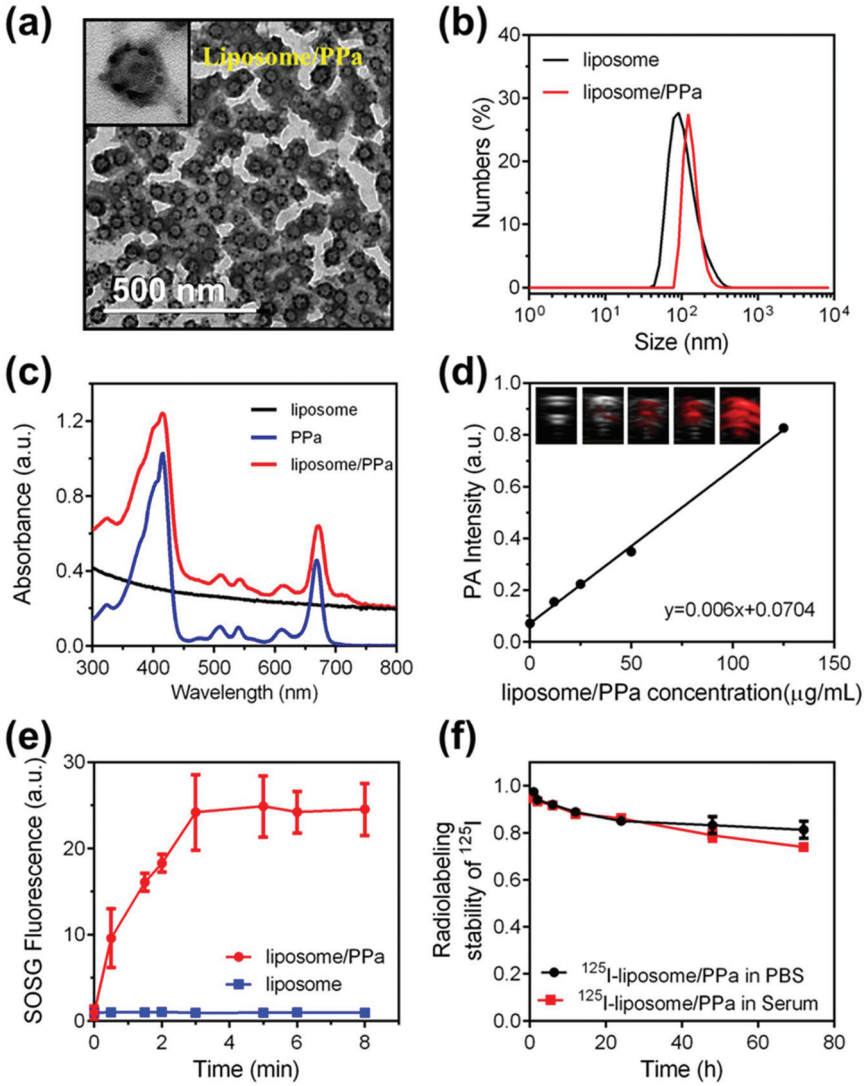

Fig. 1 Characterization of liposome/PPa. (a) A TEM image of liposome/PPa stained with phosphotungstic acid (Inset: the TEM image of a single liposome/PPa nanoparticle). (b) Hydrodynamic diameters of liposome/PPa NCPs. (c) UV–vis–NIR absorbance spectra of liposome/PPa and liposome in PBS, and PPa in chloroform, at the same PPa concentration. (d) PA imaging of liposome/PPa samples at different PPa concentrations under the excitation of a 690 nm pulsed laser. (e) Measurement of singlet oxygen production by liposome/PPa and liposome using the SOSG test. The laser power density was 0.5 W cm^{-2} for a 690 nm laser. (f) The radioactive stability of ^{125}I-liposome/PPa after incubation with PBS or serum, respectively.

intrinsic benzene ring structure of PPa, radionuclide ^{125}I could also be used to label liposome/PPa nanoparticles for small animal SPECT/CT imaging. The radioactive stability of ^{125}I-liposome/PPa nanoparticles was further investigated in mouse serum and PBS at 37 °C. It was found that ^{125}I-liposome/PPa showed excellent stability in different solutions for 24 h (Fig. 1f). Therefore, our as-prepared liposome/PPa nanoparticles possessed tri-modal imaging including PA imaging/fluorescence imaging/SPECT imaging and PDT of cancer.

For investigating cell uptake, 4T1 cells pre-incubated in a 24 well plate were incubated with liposome/PPa nanoparticles (3 μg per well of PPa) for different time points, and imaged using a confocal microscope. As expected, a strong fluorescence signal was found in the cytoplasm of the cells after 12 h of incubation, suggesting that liposome/PPa nanoparticles exhibited excellent cellular uptake *via* endocytosis (Fig. 2a). Meanwhile, liposome/PPa nanoparticle treated cells were collected for flow cytometry measurements. The results showed that the uptake of liposome/PPa nanoparticles by the cells increased with the incubation time (Fig. 2b). Before investigating the biomedical application of liposome/PPa nanoparticles, the cytotoxicity of liposome/PPa nanoparticles was evaluated by using the methyl thiazolyl tetrazolium (MTT) assay. The results showed that liposome/PPa nanoparticles exhibited excellent biocompatibility to 4T1 cells at high concentrations of 0.7–300 μg ml^{-1} of PPa (Fig. 2c). Although liposome/PPa nanoparticles showed no significant cytotoxicity, liposome/PPa nanoparticles exhibited significant concen-

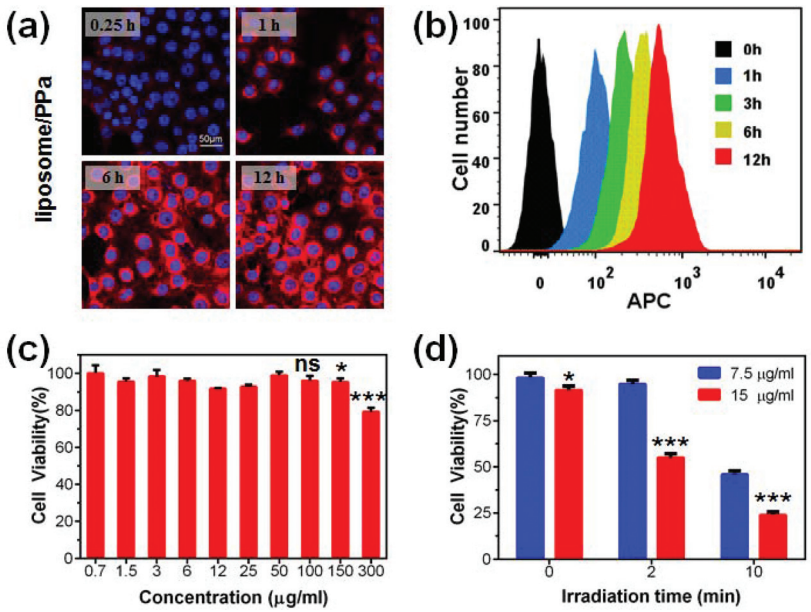

Fig. 2 *In vitro* experiments. (a) Confocal images of 4T1 cells incubated with liposome/PPa (3 μg per well of PPa) at different time points. Blue color was from the DAPI stained nucleus. The red color was from the PPa fluorescence. (b) Flow cytometry assay of PPa fluorescence intensities of 4T1 cells incubated with liposome/PPa. (c) Relative viabilities of 4T1 cells after being incubated with liposome/PPa in the dark for 24 h. (d) Relative viabilities of 4T1 cells treated with liposome/PPa (7.5 μg ml^{-1} or 15 μg ml^{-1} of PPa plus 690 nm laser irradiation (0.5 W cm^{-2})). Statistical analysis was performed using Student's two-tailed *t*-test (ns, non-significant, $*P < 0.05$, $**P < 0.01$, $***P < 0.001$).

tration dependent toxicity under 690 nm-laser irradiation. Cells incubated with different concentrations of liposome/PPa nanoparticles (7.5 μg ml^{-1} or 15 μg ml^{-1}) for 12 h were irradiated with a 690 nm laser at a power of 0.5 W cm^{-2} for 2 or 10 min, respectively. From the MTT assay, PDT using liposome/PPa nanoparticles was found to be concentration-dependent (Fig. 2d).

In order to further investigate the PDT efficiency, the liposome/PPa nanoparticle treated cells after laser irradiation were stained with Calcein-AM (green color for living cells) and propidium iodide (PI) (red color for dead cells), and then observed by confocal imaging. The results showed that strong red color was found after 10 min of irradiation, further confirming effective PDT of cancer cells using liposome/PPa nanoparticles under 690 nm-laser irradiation (Fig. 3a). Additionally, to verify the generation of ROS by liposome/PPa nanoparticles under 690 nm laser irradiation, DCFH-DA was used to probe intracellular ROS production. 4T1 cells treated with liposome/PPa nanoparticles (PPa at a dose of 15 μg ml^{-1}) for 12 h, were irradiated with a 690 nm laser at a power of 0.5 W cm^{-2} for 2 or 10 min. The DCFH-DA probe was then added to the medium containing the cells for 30 min incubation. Afterwards, the cells were imaged by confocal microscopy. A strong green fluorescence signal was observed in the cells after 2 or 10 min of irradiation compared with the control group, indicating the generation of a large amount of ROS by liposome/PPa nanoparticles under laser irradiation (Fig. 3b). On the other hand, acridine orange (AO) staining was selected to reflect the lysosomal structure. When the lysosomal membrane was destroyed, AO was deprotonated and showed green fluorescence. In contrast, AO exhibited red fluorescence in normal cells. As shown in Fig. 3c, PPa or laser only, PPa and laser or liposome/PPa nanoparticle treated cells exhibited significant red fluorescence around the cell nucleus, demonstrating that these treatments induced no obvious lysosomal structural damage in the cancer cells. However, a significant difference between the laser irradiated and non-laser irradiated liposome/PPa treated cells was found (Fig. 3c). As expected, the liposome/PPa nanoparticle treated cells exhibited green fluorescence in the cytoplasm after 690 nm laser irradiation, indicating that the ROS generated by liposome/PPa nanoparticles under 690 nm-laser irradiation could destroy the lysosomal membrane structure and induce cell death. Therefore, liposome/PPa nanoparticles could be used as excellent nanoagents for cancer PDT.

Owing to their intrinsic fluorescence and high NIR absorbance properties, as well as extra radio labelling, liposome/PPa nanoparticles could be used as contrast agents for multimodal imaging including fluorescence imaging, PA imaging and SPECT/CT imaging. Mice bearing 4T1 tumors were intravenously injected with liposome/PPa nanoparticles (10 mg kg^{-1}) and imaged *in vivo* using an animal fluorescence imaging system at different time points. As shown in Fig. 4a, liposome/PPa nanoparticles exhibited high tumor accumulation after 12 h of injection. However, the fluorescence signal at the tumor sites became weak after 24 h, indicating that liposome/PPa nanoparticles might be excreted from the body (Fig. 4a). After 48 h of observation, the major tissues

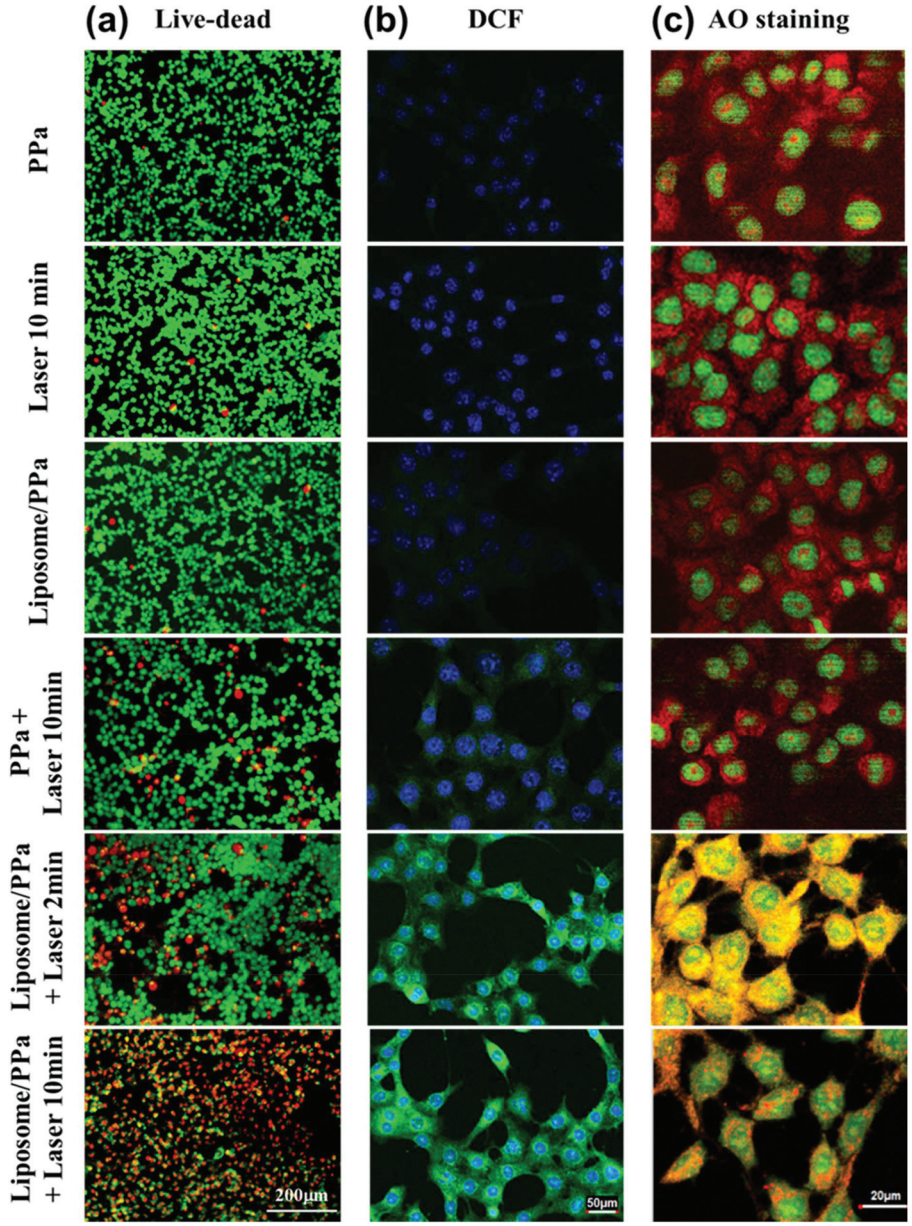

Fig. 3 (a) Confocal images of cells with different treatments stained with Calcein-AM (green spots) and PI (red spots) to differentiate live/dead cells. (b) A 2,7-dichlorofluorescin diacetate (DCFH-DA) probe was used to monitor the redox process of the cell and to detect PDT-induced intracellular ROS. (c) The membrane breaking effect of liposome/PPa on 4T1 cells under light.

including the liver, heart, spleen, kidneys and tumor were collected and imaged using a fluorescence imaging system (Fig. 4d). The results showed high tumor accumulation of liposome/PPa nanoparticles after intravenous injection. In addition to fluorescence imaging, photoacoustic (PA) imaging has also been developed for *in vivo* imaging without causing any side effect. Similar to fluorescence imaging, mice bearing 4T1 tumors were intravenously injected with liposome/PPa nanoparticles and imaged using a PA imaging system. The results showed that liposome/PPa nanoparticles with high NIR absorbance exhibited a strong PA signal at the tumor sites after 12 h of injection (Fig. 4c). After 24 h, the PA signal at the tumor sites became weak, likely owing to the excretion of liposome/PPa nanoparticles. Our obtained PA imaging data matched well with those of fluorescence imaging, further demonstrating that liposome/PPa nanoparticles could be used as multifunctional contrast agents for *in vivo* tumor fluorescence imaging/PA imaging. In order to further evaluate accurately the *in vivo* behaviors of liposome/PPa nanoparticles, radionuclide ^{125}I was selected to label liposome/PPa nanoparticles for SPECT/CT imaging (Fig. 4b). Mice bearing 4T1 tumors were intravenously injected with ^{125}I labeled liposome/PPa nanoparticles (500 μCi of ^{125}I per mouse, 10 mg kg^{-1} of PPa) and imaged using a SPECT/CT

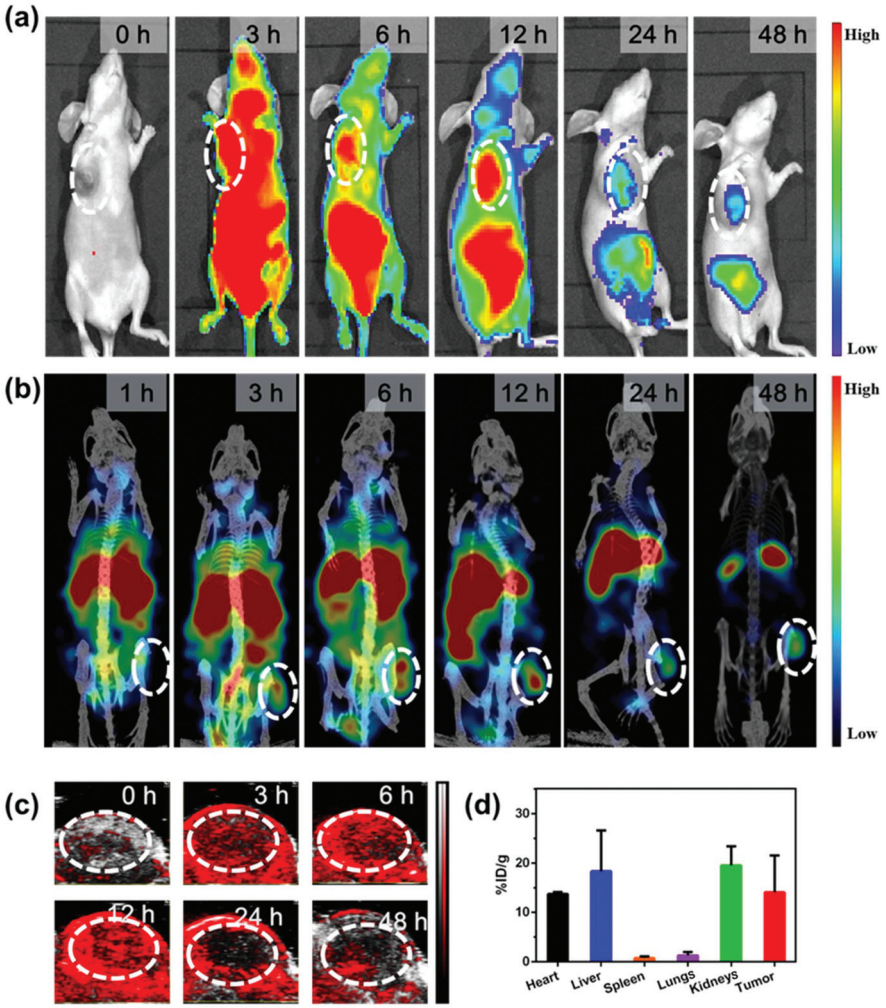

Fig. 4 *In vivo* multimodal imaging. (a) Fluorescence imaging of mice injected with liposome/PPa at different time points (0, 3, 6, 12, 24, and 48 h). (b) SPECT/CT imaging of the mice injected with ^{125}I-liposome/PPa. (c) *In vivo* PA images of 4T1 tumors of mice with intravenous administration of liposome/PPa recorded at different time intervals post-injection. (d) Quantitative analysis of *ex vivo* liposome/PPa fluorescence intensity in the major organs and tissues.

imaging system (MILabs). It was found that the radioactivity of ^{125}I-liposome/PPa nanoparticles at the tumor sites became very strong after 12 h of injection, and became weak at 24 h post injection (Fig. 4d). Additionally, the major tissues of mice after ^{125}I-liposome/PPa nanoparticle injection were collected for gamma counter measurements. The results showed high tumor accumulation of ^{125}I-liposome/PPa nanoparticles. Therefore, our prepared liposome/PPa nanoparticles could be used as excellent nanoagents for tri-modal imaging of tumors.

Motivated by the excellent tri-modal imaging data and high tumor accumulation, *in vivo* PDT using liposome/PPa nanoparticles was conducted in this work. 4T1 tumors bearing mice were taken and divided randomly into 4 groups with five mice per group: (1) injection with PBS, (2) injection of liposome/PPa nanoparticles (PPa at a dose of 10 mg kg^{-1}), (3) injection of liposome/PPa nanoparticles (PPa at a dose of 4 mg kg^{-1}) plus 690 nm laser irradiation and (4) injection of liposome/PPa nanoparticles (PPa at a dose of 10 mg kg^{-1}) plus 690 nm laser irradiation. 690 nm-laser irradiation at a power of 0.5 W cm^{-2} for 15 min was conducted 12 h post injection. During 30 days of observation, it was found that liposome/PPa nanoparticles plus laser irradiation remarkably inhibited tumor growth (Fig. 5a and c). Meanwhile, the body weight of mice with different treatments did not show any change during the whole experiment (Fig. 5b). To further evaluate the therapeutic effect, Hematoxylin and Eosin (H&E) staining of the tumor tissue from the mice with different treatments was conducted (Fig. 5d). The results showed the most severe damage to the tumor tissue of mice with liposome/PPa at a dose of 10 mg kg^{-1} under 690 nm-laser irradiation. In addition, the normal organs including the liver, spleen, kidneys, heart and lungs exhibited no obvious damage (ESI Fig. S4†).

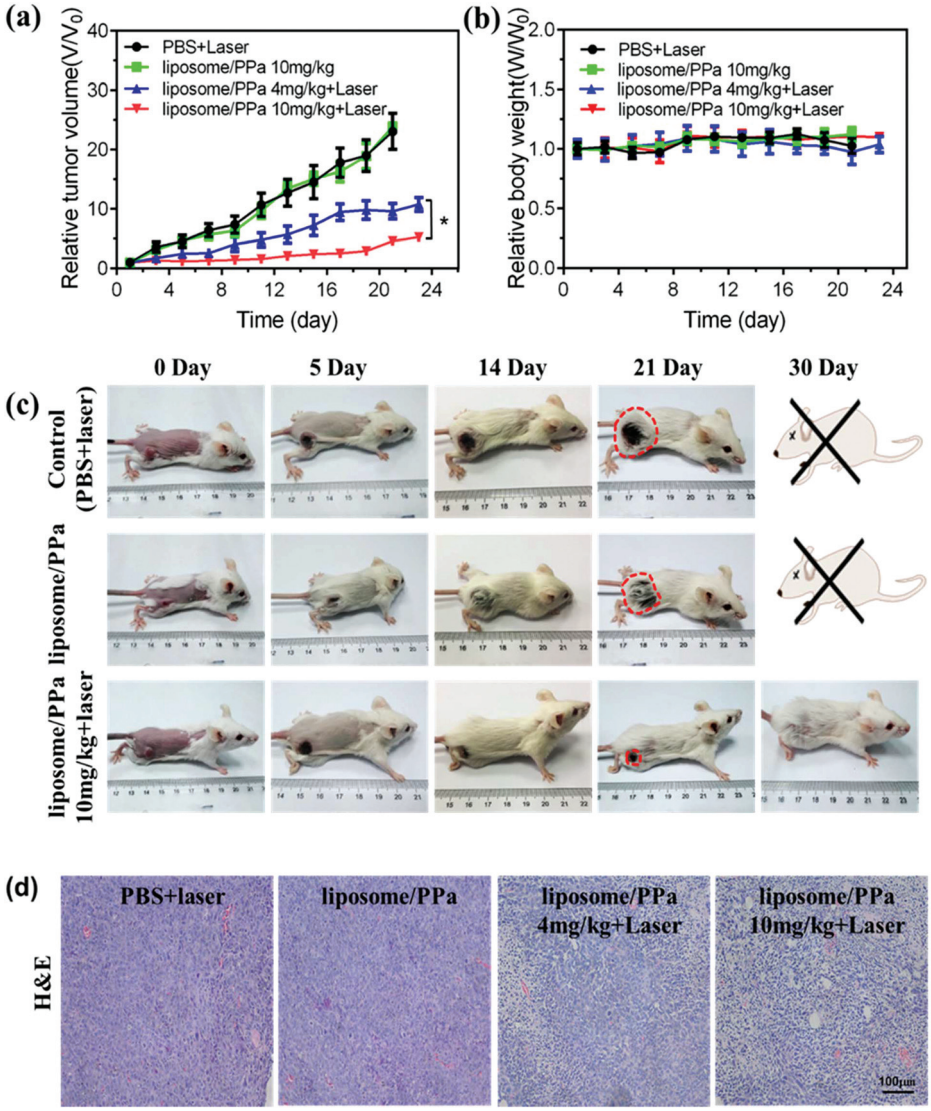

Fig. 5 *In vivo* photodynamic therapy. (a) Tumor growth curves of mice (five mice per group) after various treatments. Statistical analysis was performed using Student's two-tailed *t*-test (ns, non-significant, $*P < 0.05$, $**P < 0.01$, $***P < 0.001$). (b) The body weight changes of mice with different treatments. (c) The images of tumor-bearing mice with different treatments from day 1 to day 30. (d) H&E staining images of the tumor tissue of mice from different groups collected at day 5. The scale bar is 100 μm.

Conclusions

In summary, we have synthesized a biodegradable liposome-based drug carrier system for loading a photosensitizer, PPa, obtained from the chlorophyll of a plant extract for tri-modal imaging guided PDT of cancer. The obtained liposome/PPa nanoparticles exhibited excellent biocompatibility towards cancer cells. Under low power density laser irradiation, liposome/PPa nanoparticle incubated cells were significantly killed. At the *in vivo* level, liposome/PPa nanoparticles showed long-term blood circulation and high tumor accumulation. Utilizing the intrinsic properties and extra radiolabeling, liposome/PPa nanoparticles could be used as an excellent contrast agent for tri-modal imaging including fluorescence imaging/photoacoustic imaging/SPECT imaging. Similar to *in vitro* experiments, liposome/PPa nanoparticles significantly inhibited tumor growth owing to $^1O_2$ generation under 690 nm laser irradiation. Therefore, plant-derived PPa conjugated with liposomes showed great potential in cancer theranostics, further promoting the clinical transformation application of plant extracts.

Experimental section

Synthesis of liposome/pyropheophorbide acid (PPa) nanoparticles

To prepare liposome/PPa nanoparticles, the lipid membranes comprising DPPC, cholesterol, DSPE-mPEG$_{5k}$ and PPa were dissolved into a mixed solution of chloroform and anhydrous

methanol at a mole ratio of 3 : 1 : 2 : 0.1. The mixed solution was then blow-dried with nitrogen and dried overnight in the vacuum of a freeze dryer. After that, the obtained liposome mixture was re-dissolved in PBS solution (2 ml), and then stirred at 45 °C for one hour. Finally, the solution of the liposome mixture was squeezed through a 200 nm polycarbonate filter 10 times (Nuclepore, Whatman). Sephadex G_{100} glucan gel was used to separate liposomes and free PPa.

The hydrodynamic diameter and the morphology of liposome/PPa nanoparticles were determined using a Nanosizer ZS90 (Malvern Instruments Limited, England) and TEM (transmission electron microscopy, Hitachi, H-7650), respectively. The absorption spectra of liposome/PPa were also recorded on a UV-vis-NIR spectrophotometer (PerkinElmer).

In vitro experiments

For the culture of 4T1 murine breast cancer cells, we referred to our previously published protocol.[29] For cell uptake experiments, 8 mm^2 circular coverslips were placed in 24-well plates, and then 5×10^4 cells were seeded in each well and then incubated for 24 h. Liposome/PPa nanoparticles (3 μg per well of PPa) were added into the 24-well plates and incubated for different time points (0.25, 1, 6, and 12 h). After that, the cells were washed and fixed with paraformaldehyde, and then stained with 4′,6-diamidino-2-phenylindole (DAPI). Finally, a confocal microscope (OLYMPUS) was used to observe the distribution of liposome/PPa nanoparticles.

Besides, the cytotoxicity of liposome/PPa nanoparticles was evaluated by using the methyl thiazolyl tetrazolium (MTT) assay. 4T1 cells in 96-well plates were incubated with different concentrations of liposome/PPa for 24 h. The MTT assay was then conducted to measure the relative cell viability.

For *in vitro* PDT, the cells were first incubated in 96-well plates and then treated with liposome/PPa at 7.5 μg ml^{-1} or 15 μg ml^{-1} of PPa. After 12 h of incubation, the cells were irradiated with a 690 nm laser with a power density of 0.5 W cm^{-2} for 2 or 10 min. Meanwhile, the control group was placed in the dark. After another 3 h of incubation, the MTT assay was conducted to test the relative cytotoxicity in each group.

In order to further observe the potential toxicity of liposome/PPa plus laser irradiation, cells with liposome/PPa (15 μg ml^{-1} of PPa) plus laser irradiation were stained with Calcein-AM/PI to differentiate live and dead cells, and then imaged using a confocal microscope (Olympus). For intracellular reactive oxygen species (ROS) detection, a DCFH-DA probe was selected to monitor the cell redox process and to measure the PDT-induced intracellular ROS level. 5×10^4 Cells were seeded into a 24 well plate and then incubated with liposome/PPa at a concentration of 15 μg ml^{-1} for 12 h. After removing the incubation medium and adding the fresh medium, cells were exposed to a 690 nm-laser at a power of 0.5 W cm^{-2} for different time points (0, 2 or 10 min). After that, the irradiated cells were incubated with 10 μM per well of DCFH-DA at 37 °C for 30 minutes. Finally, DCF fluorescence was observed by confocal fluorescence microscopy. Acridine orange (AO) could only reach the nucleus through the disordered region of the dead cell membrane and was embedded in the DNA double helix of the cell, producing red fluorescence. 4T1 cells in a 24-well plate were cultured in the cell medium containing 15 μg ml^{-1} liposome/PPa for 24 h. Then the supernatant was removed and the cells were washed 3 times with the assay buffer to fully remove residual esterase. A dyeing liquid was added to the cell plate at 37 °C for 15 min.

Tumor model

Female Balb/c mice were obtained from Nanjing Peng Sheng Biological Technology Co. Ltd. All animal procedures were performed in accordance with the Guidelines for Care and Use of Laboratory Animals of Soochow University and approved by the Animal Ethics Committee of Soochow University Laboratory Animal Center. Tumor models were established according to our previously published protocols.[29]

Multimodal imaging

Mice bearing 4T1 tumor models were used for multimodal imaging including fluorescence imaging, photoacoustic imaging and SPECT/CT imaging. For *in vivo* fluorescence imaging, mice bearing 4T1 tumors were intravenously injected with liposome/PPa (10 mg kg^{-1} of PPa) and imaged using a Maestro *in vivo* optical imaging system. Similar to fluorescence imaging, the liposome/PPa treated mice were also imaged using an *in vivo* photoacoustic imaging system (Vevo LAZR) at different time points. Before SPECT imaging, the tested mice were first given gastric gavage with potassium iodide (200 μl, 1%) three times a day for a week for blocking their thyroid. For SPECT/CT imaging, the mice were intravenously injected with radionuclide ^{125}I labeled liposome/PPa at a radioactive dose of 500 μCi per mouse, and then imaged using a small animal SPECT/CT imaging system (MILabs).

In vivo PDT

20 mice bearing 4T1 tumors were divided into four groups (n = 5 per group) including (1) PBS, (2) liposome/PPa (PPa at a dose of 10 mg kg^{-1}), (3) liposome/PPa (PPa at a dose of 4 mg kg^{-1}) plus 690 nm laser irradiation and (4) liposome/PPa (PPa at a dose of 10 mg kg^{-1}) plus 690 nm laser irradiation. The tumor sizes and body weights were recorded every two days. Additionally, tumor tissues from different treated groups were collected three days post injection for H&E staining and examined using a fluorescence microscope (Olympus).

Conflicts of interest

There are no conflicts to declare.

Acknowledgements

This work was partially supported by the National Natural Science Foundation of China (31822022), the Jiangsu Natural Science Fund for Outstanding Youth Science Foundation

(BK20180094), and a Project Funded by the Priority Academic Program Development of Jiangsu Higher Education Institutions (PAPD).

References

1 A. Lichota and K. Gwozdzinski, *Int. J. Mol. Sci.*, 2018, **19**, 3533–3571.
2 X. J. Song, L. Z. Feng, C. Liang, G. S. Song and Z. Liu, *Nano Res.*, 2017, **10**, 1200–1212.
3 G. B. Yang, X. X. Gong, P. L. Qian, Z. W. Teng and Y. You, *Nano Res.*, 2015, **8**, 751–764.
4 R. D. Lin and N. F. Steinmetz, *Nanoscale*, 2018, **10**, 16307–16313.
5 Y. Liu, L. Huang and F. Liu, *Mol. Pharm.*, 2010, **7**, 863–869.
6 Y. Bao, Y. Guo, X. Zhuang, D. Li, B. Cheng, S. Tan and Z. Zhang, *Mol. Pharm.*, 2014, **11**, 3196–3209.
7 L. Z. Feng, D. L. Tao, Z. L. Dong, Q. Chen, W. M. Chen and Z. Liu, *Biomaterials*, 2017, **127**, 13–24.
8 L. Lv, Y. Jiang, X. Liu, B. Wang, W. Lv, Y. Zhao, H. Shi, Q. Hu, H. Xin and Q. Xu, *Mol. Pharm.*, 2016, **13**, 3506–3517.
9 J. Kato, Y. Li, K. Xiao, J. S. Lee, J. Luo, J. M. Tuscano, R. T. O'Donnell and K. S. Lam, *Mol. Pharm.*, 2012, **9**, 1727–1735.
10 Y. Wang, L. Dou, H. He, Y. Zhang and Q. Shen, *Mol. Pharm.*, 2014, **11**, 885–894.
11 W. L. Wan, Y. J. Lin, H. L. Chen, C. C. Huang, P. C. Shih, Y. R. Bow, W. T. Chia and H. W. Sung, *J. Am. Chem. Soc.*, 2017, **139**, 12923–12926.
12 H. Galimuhtasib, R. Hmadi, M. Kareh, R. Tohme and N. Darwiche, *Apoptosis*, 2015, **20**, 1531–1562.
13 A. Saha, S. Mohapatra, G. Das, B. Jana, S. Ghosh, D. Bhunia and S. Ghosh, *ACS Appl. Mater. Interfaces*, 2017, **9**, 176–188.
14 S. Ogasawara and H. Tamiaki, *Bioorg. Med. Chem.*, 2015, **23**, 6612–6621.
15 A. Juzeniene, *Photodiagn. Photodyn. Ther.*, 2009, **6**, 94–96.
16 A. Ferrario, D. Kessel and C. J. Gomer, *Cancer Res.*, 1992, **52**, 2890–2893.
17 W. J. Li, S. H. Tan, Y. T. Xing, Q. Liu and Z. Hong, *Mol. Pharm.*, 2018, **15**, 1505–1514.
18 D. A. Bellnier, W. R. Greco, H. Nava, G. M. Loewen, A. R. Oseroff and T. J. Dougherty, *Cancer Chemother. Pharmacol.*, 2006, **57**, 40–45.
19 A. Srivatsan, M. Ethirajan, S. K. Pandey, S. Dubey, X. Zheng, T. H. Liu, M. Shibata, J. Missert, J. Morgan and R. K. Pandey, *Mol. Pharm.*, 2011, **8**, 1186–1197.
20 X. Yu, D. Gao, L. Gao, J. Lai, C. Zhang, Y. Zhao, L. Zhong, B. Jia, F. Wang and X. Chen, *ACS Nano*, 2017, **11**, 10147–10158.
21 L. M. Song, W. Kee, K. K. Wang and A. R. Zinsmeister, *Cancer*, 2015, **82**, 421–427.
22 G. B. Yang, L. G. Xu, J. Xu, R. Zhang, G. S. Song, Y. Chao, L. Z. Feng, F. Han, Z. L. Dong, B. Li and Z. Liu, *Nano Lett.*, 2018, **18**, 2475–2484.
23 S. Jasinski, PhD thesis, Friedrich-Alexander-Universität Erlangen-Nürnberg, 2009.
24 A. Zhou, Y. Wei, B. Wu, Q. Chen and D. Xing, *Mol. Pharm.*, 2012, **9**, 1580–1589.
25 R. Mahato, W. Tai and K. Cheng, *Adv. Drug Delivery Rev.*, 2011, **63**, 659–670.
26 D. Shuai, S. Hongxi, Z. Xintong, C. Xi, C. Donghui, M. Chuanbin, G. Xiang and W. Li, *Int. J. Nanomed.*, 2018, **13**, 2199–2216.
27 J. A. Kemp, M. S. Shim, C. Y. Heo and Y. J. Kwon, *Adv. Funct. Mater.*, 2016, **98**, 3–18.
28 X. L. Liang, X. D. Li and L. J. Jing, *Biomaterials*, 2014, **35**, 6379–6388.
29 W. Chao, C. Liang, Y. Liu, X. Wang, X. Ma, Z. Deng, Y. Li and L. Zhuang, *Adv. Funct. Mater.*, 2013, **23**, 3077.